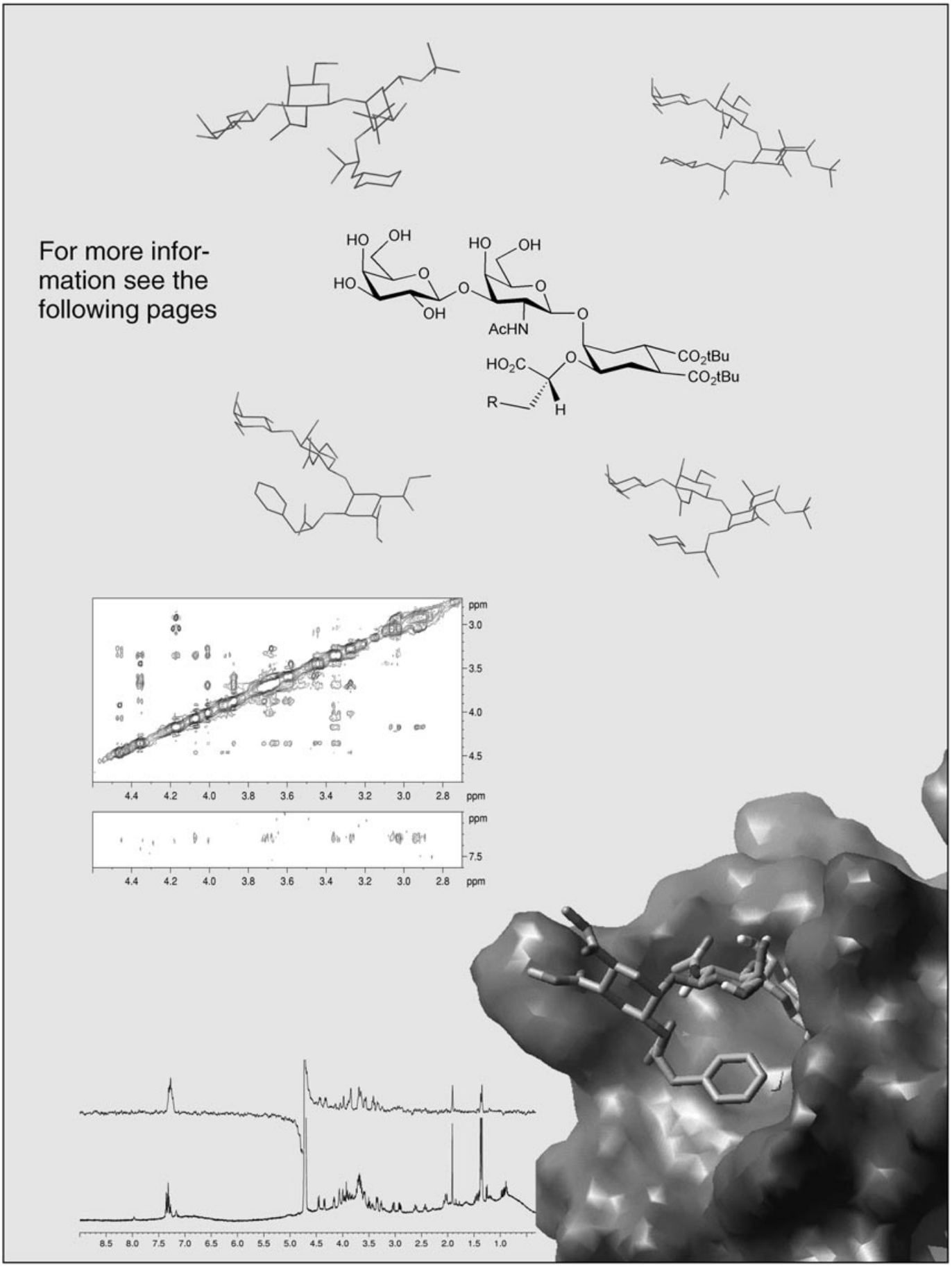

 DOI: 10.1002/chem.200400084

Intramolecular Carbohydrate–Aromatic Interactions and Intermolecular van der Waals Interactions Enhance the Molecular Recognition Ability of GM1 Glycomimetics for Cholera Toxin

Anna Bernardi,*[a] Daniela Arosio,[a] Donatella Potenza,[a] Inmaculada Sánchez-Medina,[a] Silvia Mari,[b] F. Javier Cañada,[b] and Jesús Jiménez-Barbero*[b]

Dedicated to the memory of Dr. Juan Carlos del Amo, postdoctoral fellow, killed in Madrid, in the terrorist attack of March 11th

Abstract: The design and synthesis of two GM1 glycomimetics, **6** and **7**, and analysis of their conformation in the free state and when complexed to cholera toxin is described. These compounds, which include an (*R*)-cyclohexyllactic acid and an (*R*)-phenyllactic acid fragment, respectively, display significant affinity for cholera toxin. A detailed NMR spectroscopy study of the toxin/glycomimetic complexes, assisted by molecular modeling techniques, has allowed their interactions with the toxin to be explained at the atomic level. It is shown that intramolecular van der Waals and CH–π carbohydrate–aromatic interactions define the conformational properties of **7**, which adopts a three-dimensional structure significantly preorganized for proper interaction with the toxin. The exploitation of this kind of sugar–aromatic interaction, which is very well described in the context of carbohydrate/protein complexes, may open new avenues for the rational design of sugar mimics.

Keywords: carbohydrate–aromatic interactions · carbohydrate–protein interactions · cholera toxin · glycomimetics · oligosaccharides

Introduction

Many biologically significant processes are known to be controlled in their early stages by the interaction of proteins with oligosaccharides, often in the form of glyconjugates. Thus, oligosaccharide mimics that can antagonize oligosaccharides at the protein receptor level are receiving much attention, both as tools to modulate or alter signal transmission and to be developed into drugs.[1] Our groups have been exploring this field by using the GM1 ganglioside **1a** as a model system (Scheme 1). GM1 is a membrane glycolipid which functions as the cellular receptor of two related bacterial enterotoxins, the cholera toxin (CT) and the heat-labile toxin of *Escherichia coli* (LT). Both toxins are hexameric AB5 proteins and use the GM1 headgroup pentasaccharide (o-GM1, **1b**, Scheme 1) as their molecular target to attack and penetrate the host cells. The recognition pair composed of GM1 and these two bacterial enterotoxins has been particularly well studied, both from a biochemical and a structural point of view.[2,3] This information served as the basis for the rational design of the pseudooligosaccharide **2** (Scheme 1),[4,5] which was found to be as active as GM1 in binding to CT.[4] More recently, we have reported on a group of second-generation mimics, **3**–**7** (Scheme 1),[6,7] obtained by replacing the sialic acid (NeuAc) moiety of **2** with simple α-hydroxy acids. All of these compounds show moderate to good affinity for CT (Table 1); this affinity depends critically on the configuration of the hydroxy acid stereocenter and on the nature of the substituent R (Table 1).

The design process of this series of mimics was supported by extensive NMR spectroscopy studies.[8] After the first group of three ligands (**3**–**5**, Scheme 1) was synthesized and tested, their conformation was investigated first in solution and then upon binding to the cholera toxin by using transferred nuclear Overhauser effect (TR-NOE)[9,10] measurements. It was found that CT selects a conformation similar to the global minimum of the free pseudosaccharides from

[a] Prof. Dr. A. Bernardi, Dr. D. Arosio, Dr. D. Potenza, I. Sánchez-Medina
Università di Milano—Dipartimento di Chimica Organica e Industriale e Centro di Eccellenza CISI
via Venezian 21, 20133 Milano (Italy)
Fax: (+39) 02-50314072
E-mail: anna.bernardi@unimi.it

[b] S. Mari, Dr. F. J. Cañada, Prof. Dr. J. Jiménez-Barbero
Dept. de Estructura y Función de Proteínas
Centro de Investigaciones Biológicas, C.S.I.C.
Ramiro de Maeztu 9, 28040 Madrid (Spain)
Fax: (+34) 91-5360432
E-mail: jjbarbero@cib.csic.es

Supporting information for this article is available on the WWW under http://www.chemeurj.org/ or from the author.

DOI: 10.1002/chem.200400084

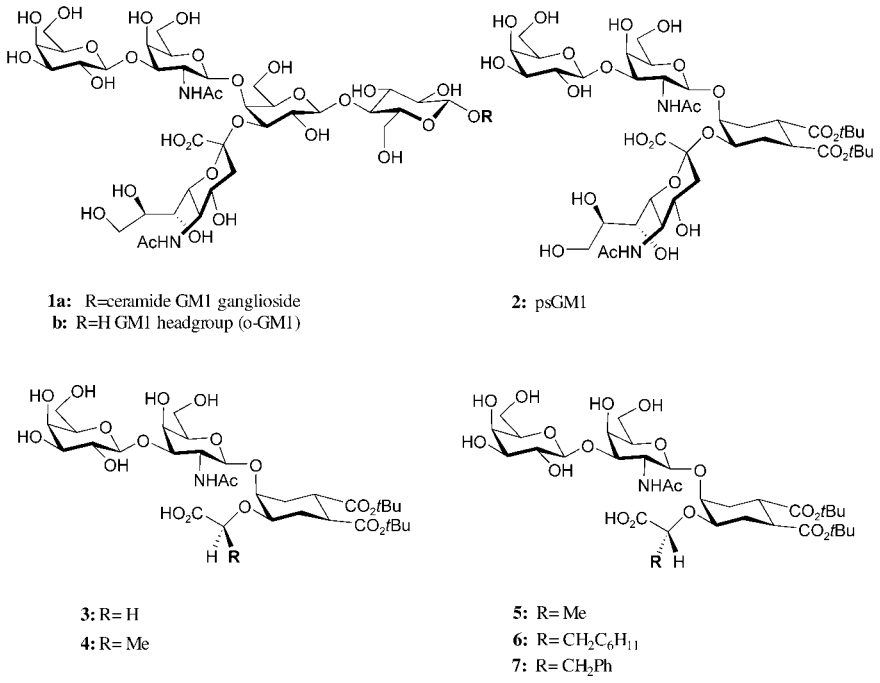

1a: R=ceramide GM1 ganglioside
b: R=H GM1 headgroup (o-GM1)

2: psGM1

3: R= H
4: R= Me

5: R= Me
6: R= $CH_2C_6H_{11}$
7: R= CH_2Ph

Scheme 1. Ganglioside GM1 and its mimics.

Table 1. CT affinity constants of the second-generation GM1 mimics **3**–**7** as determined by fluorescence titration experiments.[a]

Compound	R (configuration)	K_d [μM]	Ref.
3	H	750	[6]
4	Me (*S*)	1000	[6]
5	Me (*R*)	190	[6]
6	$CH_2C_6H_{11}$ (*R*)	45	[7]
7	CH_2Ph (*R*)	10	[7]

[a] K_d values were obtained from fluorescence intensity titrations of 0.5 μM CT solutions (in tris(hydroxymethyl)aminomethane (Tris) buffer, pH 7, room temperature) and nonlinear fitting (SigmaPlot) of data obtained in duplicate runs.

the ensemble of the presented conformations, and no evidence of major conformational distortions was obtained. In the free state the three molecules were shown to be rather flexible in the hydroxy acid region. In the bound state[8] the protein appeared to select for binding one or two side-chain conformations that could reproduce the orientation of the NeuAc carboxy group in GM1. The NMR data were interpreted with the aid of molecular-modeling techniques, which allowed workable models for the ligand:toxin complexes to be derived. These models suggested that the higher affinity of the (*R*)-lactic acid derivative **5** relative to **3** and **4** (Table 1) could result from van der Waals interactions established between its side-chain methyl group and a hydrophobic area in the toxin binding site near the sialic acid side-chain binding region of the CT/GM1 complex. This information in turn suggested that the affinity of the pseudo-GM1 binders could be improved by adding appropriate hydrophobic fragments to the framework of the (*R*)-lactic acid GM1 mimic **5**.[8] We now report on the pseudo-GM1 ligands **6** and **7**, which include a cyclohexyl group and a phenyl group, respectively. Their synthesis is described (see the Supporting Information) and detailed NMR spectroscopy and computational studies in the free state and in the complex with CT are discussed. A preliminary communication has been reported.[7]

Definitions and abbreviations: Residues of the pseudosugars **5**–**7** are defined as indicated in Scheme 2. The CHD residue is numbered as depicted in Scheme 2, to help comparison with the branching galactose unit of GM1. Glycosidic angles are defined as follows: Galβ(1→3)GalNAc: Φ = GalH1-GalC1-O1-GalNAcC3, Ψ = GalC1-O1-GalNAcC3-GalNAcH3; Galβ(1→4)CHD: Φ = GalH1-GalC1-O1-CHDC4, Ψ = GalC1-O1-CHDC4-CHDH4; hydroxy acid–CHD: Φ = C(O)-C_α-O-CHDC3, Ψ = C_α-O-CHDC3-CHDH3. The improper dihedral angle χ (see Figure 3) describes the relative orientation of the carboxy group and the CHD ring and is defined as follows: χ = C(O)-C_α-CHDC3-CHDH3. The dihedral angle θ (see Figure 4) describes the orientation of the cyclohexyl group in the hydroxy acid side chain and is defined as θ = C(O)-C_α-CH_2-CC_y.

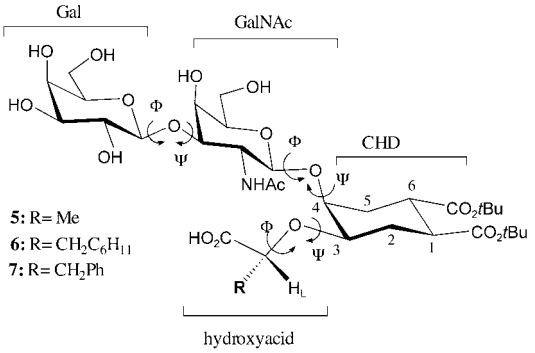

Scheme 2. GM1 mimics nomenclature, abbreviations, and definitions. Gal = galactose, GalNAc = *N*-acetyl galactosamine, CHD = cyclohexanediol, H_L = H-L in the text and other figures.

Results

Synthesis of the ligands: The synthetic pathway followed for the preparation of ligands **6** and **7** is shown in Scheme 3. The full synthetic sequence and product characterizations are reported in the Supporting Information for this paper.

Binding-affinity determination: Dissociation constants (K_d) were obtained from fluorescence intensity titrations of 0.5 μM CT solutions (in Tris buffer, pH 7, room temperature)

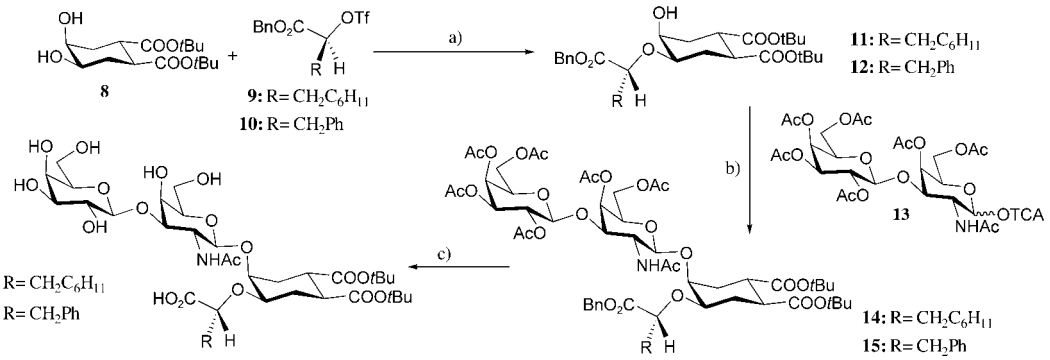

Scheme 3. Synthesis of **6** and **7**. a) Bu_2SnO, benzene, reflux; then CsF, DME, and **9** or **10**; b) **13** (0.5 equiv) and TfOH (0.05 equiv) in CH_2Cl_2, RT→reflux; c) H_2/Pd-C, MeOH; then cat. MeONa in MeOH. Bn = benzyl, DME = 1,2-dimethoxyethane, TCA = trichloroacetic acid, Tf = triflate = trifluoromethanesulfonyl.

as previously described.[7] In particular, the K_d values shown in Table 1 were obtained by nonlinear fitting (SigmaPlot) of data obtained in duplicate runs. Remarkably, the simple (*R*)-2-hydroxy-3-phenyl propionic acid (phenyllactic acid) derivative **7** showed a dissociation constant of 10 μM, which is only one order of magnitude less potent than the monovalent association of the natural ligand o-GM1 against the cholera toxin.[11] The cyclohexyl derivative **6** showed a somewhat lower affinity, with $K_d = 45$ μM; this is still better than the value obtained for the simple (*R*)-lactic derivative **5** ($K_d =$ 190 μM). This experimental fact enforces the hypothesis drawn from the previous modeling studies[8] and emphasizes the importance of setting a nonpolar group bulkier than a methyl group at the proper position. The fine details of the differences between **6** and **7** will be given below.

NMR studies of the free ligands 6 and 7: NMR spectroscopy experiments were carried out at 400 and 500 MHz at temperatures of 293–300 K. A complete assignment of the ^1H and ^{13}C NMR signals of **6** and **7** was achieved on the basis of COSY, TOCSY, HSQC, and NOESY experiments. Chemical shifts and coupling constants are reported in the Supporting Information. No changes in the NOESY spectra were noticed upon addition of calcium ions (up to 5 mM). It has been reported[12] that GM1 and other gangliosides might form complexes with calcium ions. Probably, the lack of a lipid chain, which might also affect local concentrations, may somehow influence this type of interaction in this case. For both compounds, the analysis of the vicinal proton–proton coupling constants for the six-membered rings indicates that the Gal and GalNAc chairs are in the usual $^4C1$ conformation. The diol moiety also adopts a chair conformation with the ester groups in the equatorial orientations.

The intraresidue NOE cross-peaks also support the theory that all the six-membered rings of the molecules are in chair conformations (see below and Tables 2 and 3).

Table 2. Principal NOE contacts for compound **6** in the free state and bound to cholera toxin. The distances *r* (±10%) are estimated according to a full-matrix relaxation approach.[32] The intraresidue Gal and GalNAc H-1/H-3 and H-1/H-5 contacts were taken as internal references.[a]

Proton pair		Observed intensity free state	Deduced *r* [Å]	Observed intensity bound state	Deduced *r* [Å]
H-1 GalNAc	H-4 CHD	strong	2.4	strong	2.4
	H-L	n.o.[a]	>3.5	n.o.[a]	>3.5
H-1 Gal	H-3 GalNAc	strong	2.4	strong	2.4
H-3 CHD	H-L	medium	2.7	strong	2.5
	CH_2[b]	strong		strong	
	H-2ax CHD	n.o.[a]		very weak	
H-L	H-2eq CHD	weak	2.9	medium-strong	2.7
	H-3 CHD	medium	2.6	strong	2.5
	H-4 CHD	very weak	3.1	very weak	3.2
	H-2ax CHD	n.o.[a]	>3.5	very weak	3.3
H-4 CHD	H-1 GalNAc	strong	2.5	strong	2.5
	H-L	n.o.	>3.5	weak	3.2

[a] ax = axial, eq = equatorial, n.o. = no observable NOE contact. [b] CH_2 and H-5ax CHD are isochronous.

Vicinal $J_{5,6}$ couplings for the hydroxymethyl groups could be measured for **6** and **7**. The coupling values were between 7.5–9 Hz for both the Gal and GalNAc residues, in agreement with a *gt*:*tg* equilibrium of the ω torsion angle, as is usually the case for these Gal-type sugars.[13]

The conformation of oligosaccharides is defined by the Φ and Ψ torsion angles around the glycosidic linkages (Scheme 2). For **6** and **7**, the rotation around the ether linkage in the hydroxy acid side chain must also be described. Φ,Ψ definitions can be extrapolated from the glycosidic bond convention and defined as described in Scheme 2. Experimental information on these geometrical parameters can be gathered by using NOE measurements.[14] Specifically, selective 1D NOESY and 2D T-ROESY[14] experiments were carried out that provided experimental interproton distances.

These, in turn, allowed the conformation equilibria present in solution to be profiled and average molecular conformations to be derived (Tables 2 and 3).

The relationship between NOE signals and proton–proton distances is well established[15,16] and can be worked out at

Table 3. Principal NOE contacts for compound **7** in the free state and when bound to cholera toxin. The distances r (±15%) are estimated according to a full-matrix relaxation approach.[32] The intraresidue Gal and GalNAc H-1/H-3 and H-1/H-5 contacts were taken as internal references.

Proton pair		Observed intensity free state	Deduced r [Å]	Observed intensity bound state	Deduced r [Å]
H-1 GalNAc	H-4 CHD	strong	2.4	medium-strong	2.5
	H-L	n.o.	>3.5	n.o.	>4.0
H-1 Gal	H-3 GalNAc	strong	2.4	strong	2.4
Ph	H-1 GalNAc	medium	2.8	medium	2.8
	H-L	medium	2.7	medium	2.7
	H-4 CHD	medium	2.8	medium	2.8
	H-6 GalNAc	weak	3.1	medium	2.8
	H-3 GalNAc[a]	medium	2.8	medium	2.8
	H-5 GalNAc	medium	2.8	medium	2.8
H-L	H-3 CHD[a]	strong	2.3	strong	2.3
	H-2eq CHD	strong	2.4	strong	2.4
	H-1 CHD	weak	3.0	weak	3.2
H-4 CHD	H-1 GalNAc	strong	2.5	strong	2.5
	H-L	strong	>3.5	weak	3.2
	H-1 GalNAc	strong	2.5	strong	2.5
	H-L	n.o.	>3.5	weak	3.2

[a] H-3 GalNAc and H-3 CHD are isochronous.

least semiquantitatively by using a relaxation matrix.[16] The NOE intensities reflect the conformer populations, and therefore information on the population distributions in free solution can be obtained by focusing on the key, mutually exclusive NOE interactions that characterize the different possible conformations.[17]

At 400 MHz all the cross-peaks observed in the NOE spectra of **6** and **7** were very weak. The $\omega\tau_c$ value is close to 1.1, which provides an almost zero longitudinal NOE contact (τ_C is the overall correlation time). Although some initial information could be derived from T-ROESY spectra, many crucial proton signals (for example, H-L and H-2 GalNAc) were basically isochronous; this prompted us to a 500 MHz analysis. At 293 K, the corresponding NOESY spectra (Figures 1 and 2) were good enough to extract the observed cross-peaks, which are reported in Tables 2 and 3.

The orientation around the Galβ(1→3)GalNAc linkage can be defined[8,18] by the NOE contact observed between the anomeric proton of galactose, H-1 Gal, and the protons on the GalNAc moiety, especially H-3, H-4, and H-2. The H-1 Gal/H-3 GalNAc cross-peak is very strong for both **6** and **7** (see Tables 2 and 3), with an interaction similar to or even stronger than the corresponding intraresidue H-1 Gal/H-3 Gal and H-1 Gal/H-5 Gal cross-peaks. As we have already described for **3**–**5**,[8] the H-1 Gal/H-3 GalNAc distance obtained from the NMR spectroscopy data (approximately 2.4 Å) can be correlated with one major orientation around the Galβ(1→3)GalNAc Φ/Ψ torsion angles. This region corresponds to the global minimum *syn* conformation, characterized by Φ/Ψ values of around 60°/−20°.

A similar situation occurs for the GalNAcβ(1→4)CHD moiety, with a similar NOE pattern.[8,18] In fact, only the very strong interresidue H-1 GalNAc/H-4 CHD cross-peak is observed; this cross-peak corresponds to a H-1 GalNAc/H-4 CHD distance of 2.5±0.2 Å. The average conformation in solution for this linkage corresponds to the global minimum *syn* conformer, characterized by Φ/Ψ values of around 50°/20°. Conformers in the *anti*-Φ or *anti*-Ψ regions of both glycosidic linkages with populations above 5% would give rise to exclusive H-1 Gal/H-2, H-4 GalNAc and/or H-1 GalNAc/H-5ax, H-5ax CHD NOE contacts that are not observed in these cases.

Regarding the orientation of the acetamide moiety[18] of both **6** and **7**, the cross-peak of the methyl group with the corresponding H-2 GalNAc proton is a very weak, and no cross-peaks to either H-1 or H-3 GalNAc are observed. Therefore, these observations are in agreement with a major orientation in solution with the methyl group pointing out of the pyranoid ring with an *anti*-like relationship with the C-2 atom.

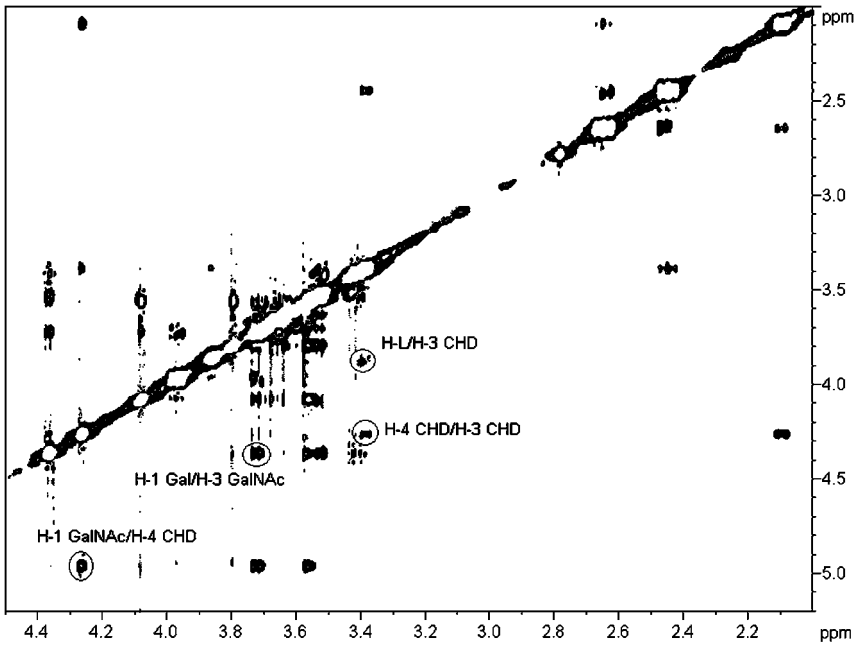

Figure 1. 500 MHz NOESY spectrum of **6** in D_2O at 293 K.

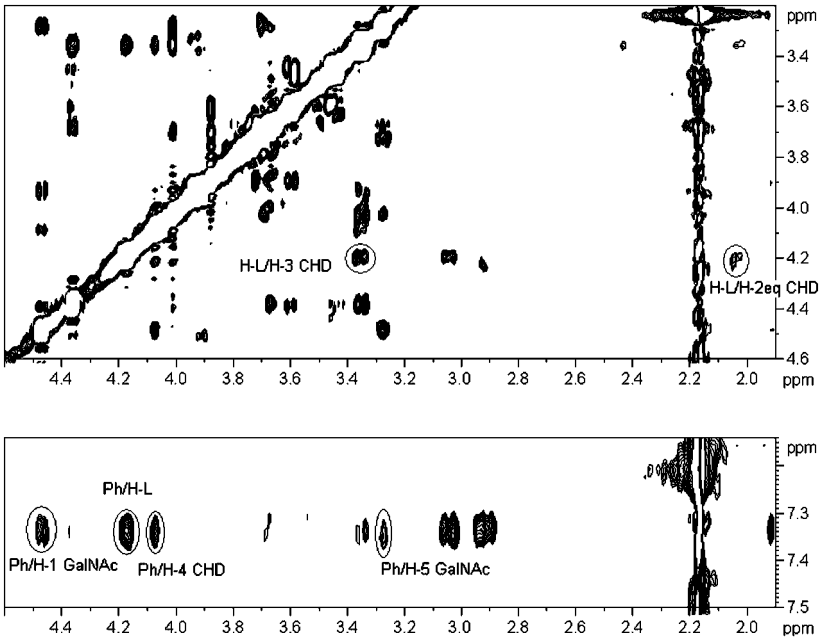

Figure 2. Fragments of the 500 MHz NOESY spectra of **7** in D_2O at 300 K, from which the orientation of the side chain is deduced. The NOE contacts for H-L (top) and for the aromatic protons (bottom) are indicated.

Thus, all data so far concur to describe the "upper" portion of both **6** and **7** as a pseudotrisaccharide with relatively little flexibility, which can be described by oscillations around one single major conformation. This is the same situation observed for all the GM1 mimics synthesized so far,[8] and for the Galβ(1→3)GalNAcβ(1→4)Gal fragment of o-GM1 itself.[19]

The additional torsional degrees of freedom available for **6** and **7**, correspond to the hydroxy acid side-chain bonds. Due to the absence of anomeric effects, the ether linkage that connects the CHD ring to the hydroxy acid moiety is more flexible than the interglycosidic linkages described so far. The NOE contacts observed in this region can arise form multiple combinations of Φ,Ψ values that happen to determine similar through-space proton–proton interactions for the reporter H-L. Thus, the experimental inter-proton distances generated by NMR spectroscopy analysis can be analyzed more conveniently by using the improper dihedral angle descriptor χ(C(O)-C_α-CHDC3-CHDH3), which is defined in Figure 3, and univocally describes the orientation of H-L (and of the hydroxy acid carboxy group) relative to the CHD ring. In principle, three idealized staggered orientations can be drawn across the ether connector (Figure 3); these can be identified as *anti*-χ, $(-g)$-χ, and $(+g)$-χ and they give rise to specific interactions between H-L and the protons on the C-3, C-2 and C-4 carbon atoms of the CHD ring. The major orientation(s) of the hydroxy acid relative to the CHD ring can thus be defined by focusing on the NOE cross-peaks for the H-L proton to H-3, H-4, H-2eq, and H-2ax of CHD (Tables 2 and 3). Further information on the mobility of the side chain and on its conformation(s) can be gathered from the NOE contacts observed for the R side-chain substituent.

For the cyclohexyl derivative **6**, medium and weak NOE contacts are observed between H-L and the key CHD protons (see Table 2). Nevertheless, the NOE intensity of the H-L/H-3 CHD cross-peak is higher than that of the H-L/H-2eq CHD connectivity and also stronger than the H-L/H-4 CHD one. The H-L/H-1 GalNAc and H-L/H-2ax NOE cross-peaks are also negligible. In turn, the cyclohexyl moiety of the side chain only displays weak cross-peaks to its vicinal H-3 CHD proton. No cross-peaks are observed

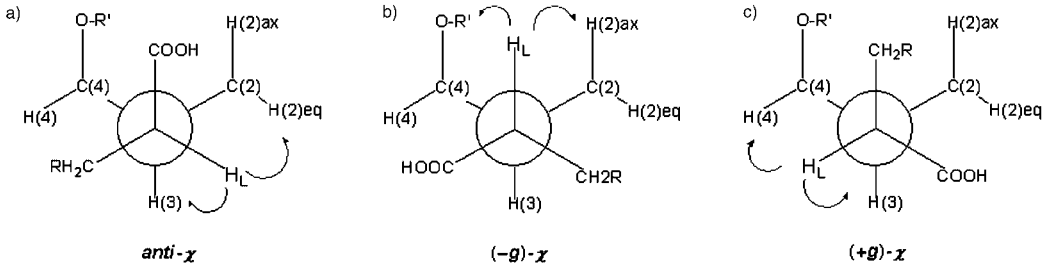

	a) *anti*-χ	b) $(-g)$-χ	c) $(+g)$-χ
NOE contacts expected for proton H-L	H-L / H-3 CHD	H-L / H-2ax CHD	H L / H-3 CHD
	H-L / H-2eq CHD	H-L / H-1 GalNAc	H L / H-4 CHD

Figure 3. Newman projections along the ether linkage between the CHD ring and the hydroxy acid moiety. The exclusive NOE contacts expected for H-L in each rotamer are shown. Each of these projections may correspond to multiple Φ,Ψ combinations. χ = the improper dihedral angle. See text for further details.

between the cyclohexyl side chain and H-2eq or H-4 CHD. The absence of cross-peaks between H-L and H-1 GalNAc and the very weak intensity of those between H-L and H-4 CHD and between H-L and H-2 CHD are consistent with a very flexible side chain and indicate that probably all three staggered rotamers depicted in Figure 3 are contributing to the equilibrium.

For the conformation analysis of **7**, the key NOE contacts that allow the conformation equilibrium present in solution to be described were obtained from NOESY and T-ROESY experiments carried out at 500 MHz and 300 K. Several interresidual cross-peaks were observed. As described above for **6**, the major arrangement of the hydroxy acid side chain can be defined by focusing on the NOE contacts between H-L and the CHD protons. In this case, important information is also obtained from the through-space interactions between the aromatic protons and the CHD and GalNAc residues (Figure 2, Table 3). The H-L proton shows NOE cross-peaks of strong intensity with H-2eq and H-3 CHD (with corresponding distances of 2.4 and 2.3 ± 0.1 Å, respectively), while no cross-peaks are observed between H-L and H-4 CHD (Figure 2a, Table 3). This pattern, which is markedly different from what was measured for **6**, is in agreement with one major *anti*-χ orientation (Figure 3) between the carboxyl group and the H-3 CHD proton. In addition, the aromatic protons also show clear cross-peaks to a variety of protons (Figure 2b, Table 3) located not only on the CHD moiety (H-4), but also on the α face of the GalNAc residue (H-1, H-3, and H-5, Figure 2b). Thus, it appears that in the major solution conformation of **7** the phenyl moiety stacks below the GalNAc residue.

Collectively, these experimental data allow us to conclude that the phenyllactic derivative **7** is significantly less flexible in the hydroxy acid fragment than the cyclohexyllactic analogue **6** and suggest that a single conformation of the hydroxy acid chain can describe the conformational properties of **7** in aqueous solution. Importantly, the origin of this conformation lock appears to be intramolecular van der Waals and CH–π interactions between the aromatic ring and the GalNAc residue; this may be described as hydrophobic packing. These interactions are not so favorable in **6** where the cyclohexyl ring obviously differs from the phenyl moiety in its electronic and geometrical features. The importance of carbohydrate–aromatic interactions for the molecular recognition of oligosaccharides by the binding sites of proteins has been well documented.[20–24] Here, we present clear evidence of the importance of this type of interaction for favoring a given type of three-dimensional structure.

Computational models of **6** and **7** were generated by using previously established protocols (MC/EM conformation searches and MC/SD molecular-dynamics simulations, AMBER* force field augmented by the Kolb parameters[25] for hydroxy acids, GB/SA water solvation) and compared to the experimental results. The calculations showed that the Gal–GalNAc–CHD fragment of both molecules is populating the *syn* conformation for both glycosidic linkages. Minima were located at φ/ψ values of 50°/0° for the Gal–GalNAc linkage and 25°/30° for the GalNAc–CHD linkage. By contrast, and in agreement with the experimental data discussed above, the computational description of the hydroxy acid side chain differs significantly for the two molecules. For **6**, MC/EM calculations located three conformers within 1 kcal mol^{-1} of the global minimum, at $\chi = 150$, 65, and 39° (Figure 4a and Table 4). MC/SD dynamics showed that the molecule is highly flexible along the variable χ angle and continuously populates an ample region with χ varying from 40–160° plus a secondary low-energy region at $\chi = -60°$ (Figure 4b). The presence of this extensive conformation equilibrium agrees with the experimental observation.

MC/EM calculations also showed that the side chain of **7** is significantly less flexible than that of **6**, although computa-

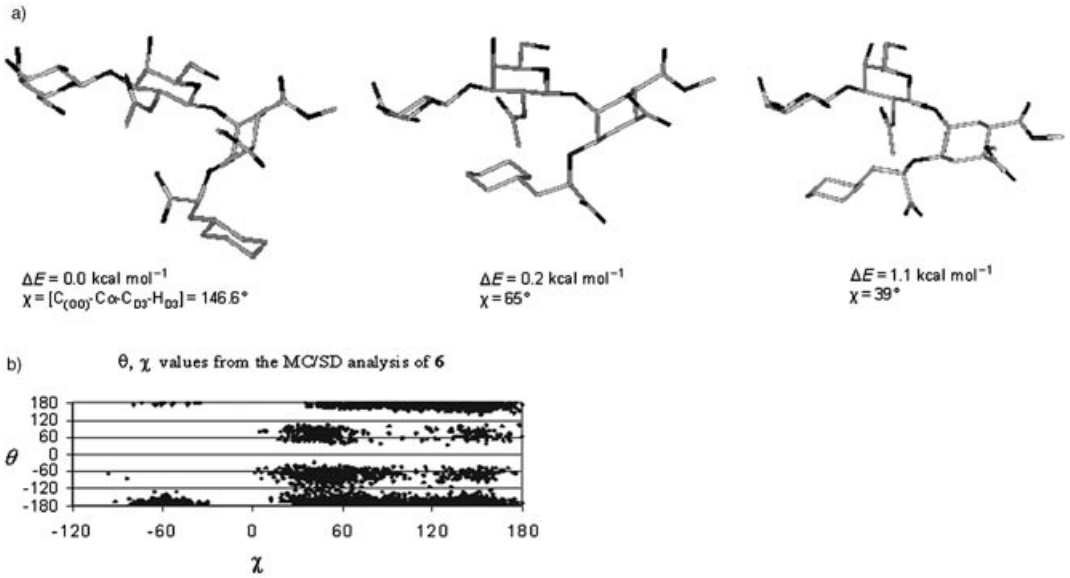

Figure 4. Conformation analysis of **6**. a) Low-energy conformations within 1.2 kcal mol^{-1} of the global minimum. b) MC/SD dynamics simulations (5 ns). The improper dihedral angle, χ, is plotted against the dihedral angle, θC(O)-C_α-CH_2-CC_γ.

Table 4. Three different conformation (conf.) families were found by an MC/EM[a] conformation search, each with a different value of the improper angle, χ ($\Phi = C_{(OO)}$-C_{α}-O-C_{D3}; $\chi = C_{(OO)}$-C_{α}-C_{D3}-H_{D3}). The key interatomic proton–proton distances are outlined.

	Distances [Å]		
	conf. 1 ($\Delta E = 0.0$ kcal mol^{-1}, $\chi = 146.6°$)	conf. 2 ($\Delta E = 0.2$ kcal mol^{-1}, $\chi = 65°$)	conf. 3 ($\Delta E = 1.1$ kcal mol^{-1}, $\chi = 39°$)
H-L/H-3 CHD	2.51	2.81	2.42
H-L/H-2eq CHD	2.25	3.92	4.24
H-L/H2ax CHD	3.39	4.49	4.47
H-L/H-4 CHD	4.39	3.22	2.47
H-L/H-1 GalNAc	4.36	3.71	2.81
H-1 GalNAc/H-4 CHD	2.69	2.24	2.31

[a] 10000 steps of MC/EM with the H_2O GB/SA solvent model and the Amber* force field were employed.

tionally the restriction of mobility is mostly confined to the orientation of the phenyl ring, which is always calculated to stack either with the Gal or the GalNAc ring (Figure 5). Two energetically equivalent orientations of the carboxyl group were calculated, with $\chi \approx 150°$ (*anti*-χ) and $\chi \approx 60°$ ((+)*g*-χ; Figure 5a and b). However, in this case, the NMR experimental data (see above) allows us to conclude that only one major orientation of the side chain, corresponding to the *anti*-χ conformation, is in fact present. The best fit with the NOE data is represented by a conformation found near the global minimum, as shown in Figure 5c. Based on these data, ligand **7** appears to be preorganized for toxin binding, in contrast with the conformational behavior of its aliphatic analogue **6**, which is fairly flexible.

It is interesting to note that the stacking effect between the aromatic ring and the sugars is somewhat "understood" by the molecular mechanics computations, which most likely "see" it as a solvation effect (the hydrophobicity of the ring) combined with a positive van der Waals interactions between the phenyl group and the α face of the sugars. This latter interaction appears to be precluded to the cyclohexyl substituent for steric reasons.

NMR studies of the CT complexes: NMR experiments, including TR-NOESY[9,10] and saturation transfer difference (STD),[26–28] were performed to deduce the bound conformations of **6** and **7** to the CT B pentamer. As previously shown, for ligands which are not bound tightly and exchange between the free and bound states at a reasonably fast rate, the TR-NOESY experiment provides an adequate means for determining the conformation of the bound ligand.[9,10] As mentioned above (Table 1), the present systems bind in the micromolar range to CT and thus can properly be studied by this technique. The addition of cholera toxin to a D_2O solution of **6** and **7** induced broadening of the resonance signals in the ^{1}H NMR spectrum, a result indicating that binding occurs (Figures S1 and S2 in the Supporting Information). TR-NOESY experiments were performed on the ligand/CT samples at different mixing times and with different ligand to toxin molar ratios (25:1 to 50:1). Negative cross-peaks were clearly observed at 300 K, as expected for ligand binding.

For the phenyllactic acid based ligand **7**, the cross-peak pattern is similar to the one described above for free **7** in aqueous solution. Indeed, the same set of interresidue cross-peaks with basically identical intensities (relative to the intraresidual contacts) were observed (Table 3). The orientation around the Galβ(1→3)GalNAc and GalNAcβ(1→4)CHD fragments is unchanged upon binding, as deduced by the corresponding H-1 Gal/H-3 GalNAc and H-1 GalNAc/H-4 CHD cross-peaks. The orientation of the phenyllactic acid moiety relative to the GalNAc and CHD residues is also almost identical to that observed in the free state, as shown by the H-L/H-2eq CHD, H-L/H3 CHD, and aromatic/H-1, H-3, H-5 GalNAc short contacts (Figure 6, Table 3). TR-ROESY experiments allowed spin-diffusion effects to be excluded for these key cross-peaks.[29]

For **6**, TR-NOESY experiments were also performed at a 32:1 ligand/receptor molar ratio. Negative cross-peaks were clearly observed at 300 K, both at 400 and 500 MHz, a result indicating ligand binding (Table 2). In this case, the analysis

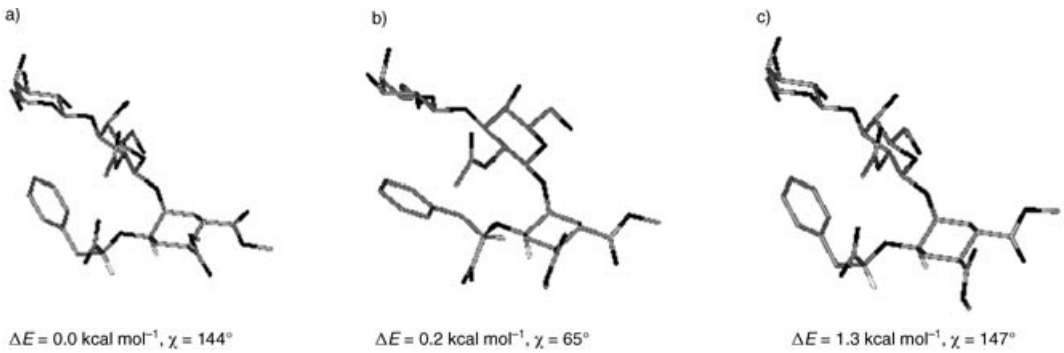

Figure 5. Two major conformation families, a and b, were found for the side chain of **7** by the MC/EM conformation search. They are characterized by a different value of the improper torsional angle, χ. According to the experimental results, only the *anti*-χ conformation ($\chi \approx 150°$) is found in solution. The best fit with the NOE data is obtained with conformer c, which belongs to the a family.

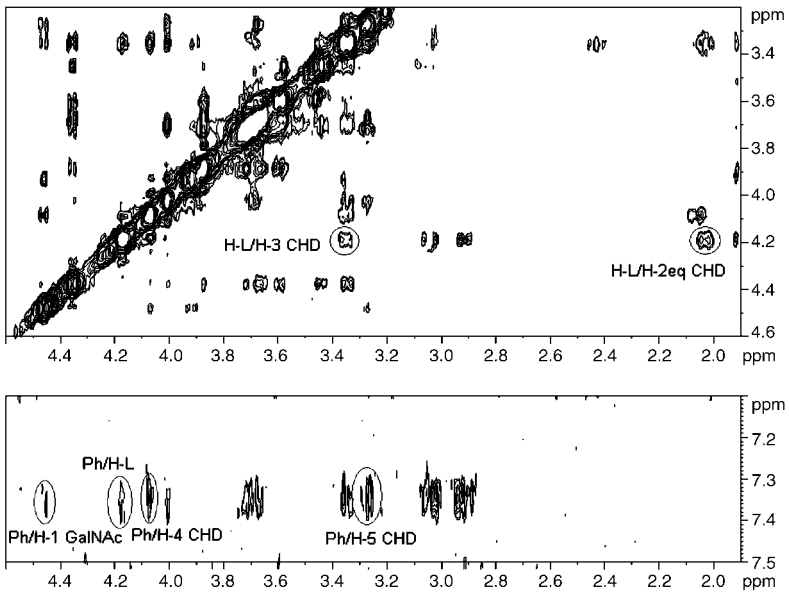

Figure 6. TR-NOESY spectrum of **7** bound to CT (solvent D_2O, 293 K).

of the cross-peaks shows that, out of the conformation equilibrium observed in the free state, one main conformation, which features an *anti*-type relationship of the carboxyl group to the H-3 CHD proton (*anti*-χ in Figure 3), is selected for binding. In fact, cross-peaks between H-L/H-2eq CHD and H-L/H-3 CHD were observed (Figure 7) that agreed with the conformation selection of the *anti*-χ rotamer ($\chi \approx 150°$). A minor proportion of a *gauche*-χ rotamer cannot be discarded, as indicated by the presence of a very weak H-L/H-4 CHD TR-NOESY cross-peak.

Finally, in order to map the binding epitope of the glycomimetics bound to the cholera toxin, 1D STD NMR experiments were also performed.[26–28] For **7**, the difference spectrum showed that the aromatic protons, together with H-4 Gal and H-6 Gal, give rise to the most prominent STD signals (Figure 8). Thus, it can be inferred that this region (aromatic ring and Gal moiety) of the glycomimetic is in more intimate contact with the toxin binding site. Additionally, the resonance signals of H-3 and H-1 Gal, H-1 GalNAc, and H-4 CHD also appeared in the difference spectrum but with smaller intensities. The weakest STD signals were observed for the CHD moiety protons, except for H-4, a result indicating that this part of the molecule is not involved in the molecular recognition process (Figure 8) to a significant extent.

The STD spectrum of the CT/**6** mixture (Figure 9) also allowed the binding epitope to be deduced. Resonance signals belonging to the Gal moiety (H-1, H-2, H-4, H-5, H-6) were evident in the difference spectrum. Additional peaks for H-1, H-4, and H-5 GalNAc were also clearly observed. However, those belonging to the CHD ring and to the pendant cyclohexyl moiety were rather weak, or basically nonexistent, including the H-3 CHD and H-4 CHD protons (see Figure 9). This indicates that these moieties establish only marginal interactions with the protein, in contrast to the aromatic ring of the phenyllactic derivative **7**.

As a final step, a three-dimensional model of the complex structures was obtained by performing MC/EM calculations within the binding site of the LT toxin, according to the procedure already described for the lactic acid analogues.[8] The corresponding views are depicted in Figure 10. It clearly appears that the phenyl ring in the LT/**7** complex (Figure 10a) is calculated to be in close proximity to the protein binding site. On the contrary, and in accordance with experimental observations, the cyclohexyl ring in LT:**6** projects away from the protein surface (Figure 10b).

Dynamics simulations (MC/SD) also showed that the phenyl ring of **7** is locked between the protein and the GalNAc ring (see Figure S3 (animated gif file) in the Supporting Information). A clear intramolecular carbohydrate–ar-

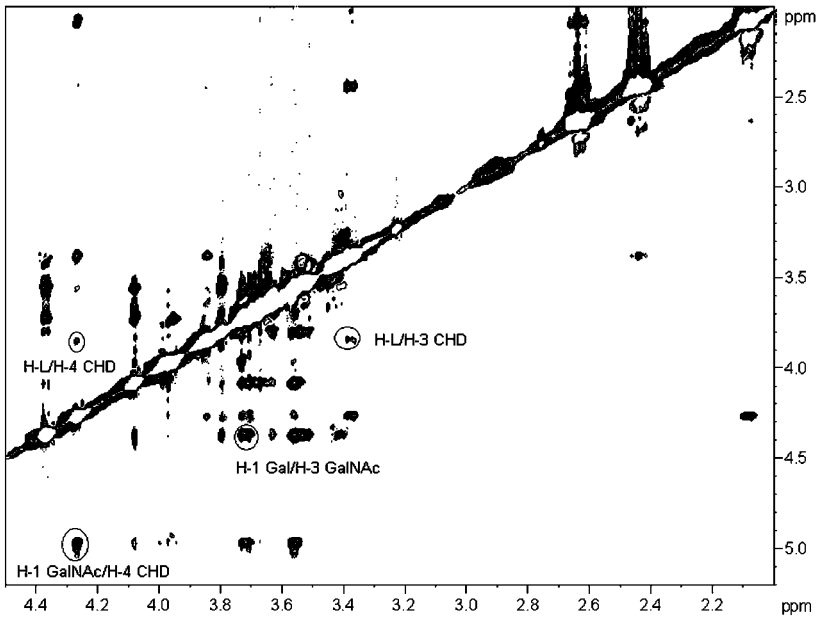

Figure 7. TR-NOESY spectrum of **6** bound to CT (solvent D_2O, 300 K).

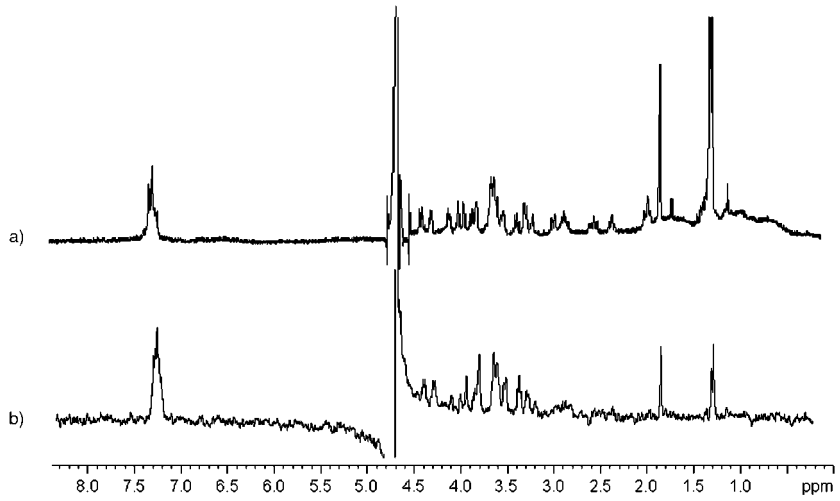

Figure 8. a) Reference 1D 1H NMR spectrum of **7** with CTB5 (ratio 25:1) in D_2O at 300 K. b) STD spectrum with 1 s presaturation of the protein envelope protons. Ligand proton signals are evident in the aromatic region. Protons are those belonging to the Gal moiety (H-4 and H-6). H-1 GalNAc, H-1 Gal, H-4 CHD, and H-3 GalNAc are also clearly visible, while the other protons of the CHD unit do not appear in the STD spectrum.

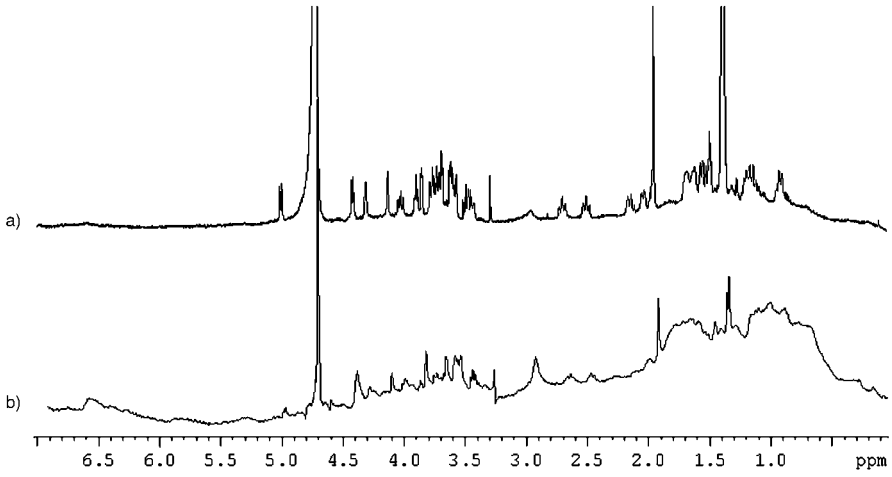

Figure 9. a) Reference 1D 1H NMR spectrum of **6** with CTB5 (ratio 32:1) in D_2O at 298 K. b) STD spectrum with 2 s presaturation of the protein envelope protons. Protons belonging to the GalNAc and Gal moiety (H-1 GalNAc, H-1 Gal, H-4 GalNAc, H-2 GalNAc, H-4 Gal, H-6 GalNAc, H-6 Gal, H-5 GalNAc, H-5 Gal, and H-2 Gal) are clearly visible.

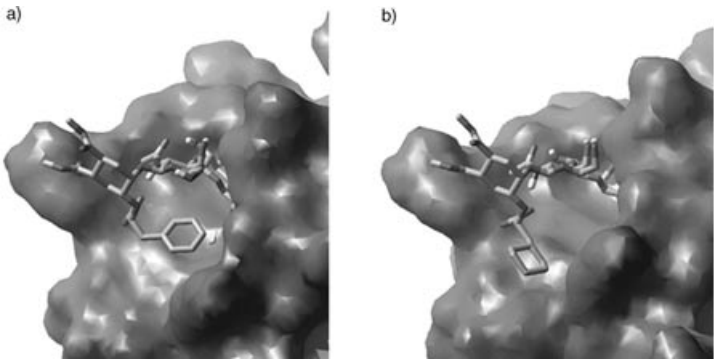

Figure 10. a) Molecular model (MC/EM, Amber*, H_2O, GB/SA, best fit with experimental data for **7**). b) Molecular model (MC/EM, Amber*, H_2O, GB/SA, lowest energy conformer for **6**).

omatic stacking interaction takes place and locates the phenyl ring in the proper position to establish additional contacts with the hydrophobic patch in the protein. The typical Gal–toxin interaction, which defines the structure of cholera toxin complexes, is also evident.

In contrast, in the LT/**6** complex the cyclohexyl ring appears to display more flexibility even in the bound state, with the Gal moiety establishing the major contacts with the toxin. No stacking of the GalNAc moiety with the aliphatic cyclohexyl side chain takes place. The cyclohexyl ring appears to move in and out of the toxin binding side and to sample at least two different orientations relative to the protein cavity (see Figure S4 (animated gif file) in the Supporting Information).

Discussion

All the known structural data on the complexes formed between CT and GM1 or the pseudo-GM1 mimics **2**–**5** show that the principal interactions between the protein and the (pseudo)carbohydrate ligands are established through the nonreducing end galactose unit and the carboxy group of the NeuAc residue (in **1** and **2**) or of the surrogate hydroxy acid (in **3**–**5**). NMR and computational studies performed on the complexation of **3**–**5** by CT have suggested that additional van der Waals interactions can be gained by lipophilic substituents on the (*R*)-hydroxy acid side chain,[8] which, in the bound conformation of the ligand, can extend towards a hydrophobic area of the toxin binding site close to the region that accommodates the sialic acid side chain in the CT/GM1 complex.[3] The present work shows that the pseudo-GM1 ligands **6** and **7**, which include an (*R*)-cyclohexyllactic acid fragment and an (*R*)-phenyllactic acid fragment, respectively, do indeed display stronger affinity for CT than **5**.

Although the two ligands described in this paper are similar in nature and activity, a detailed analysis of their behavior in solution and in the binding site of the cholera toxin reveals striking differences, both in terms of conformational flexibility and of binding mode. Intra- and intermolecular in-

teractions among the different residues strongly modulate the conformational features of these molecules in solution and when bound to the toxin. The major differences between **6** and **7** may be ascribed to the presence of an intramolecular aromatic–carbohydrate interaction in the phenyllactic acid derivative **7** that strongly biases its conformational behavior by severely restricting its conformational freedom. This conformational constraint is lacking in the cyclohexyllactic acid derivative **6**, which behaves similarly to the lactic acid derivative **5** in terms of flexibility and preferred orientations of the hydroxy acid side chain. As a result of the conformation lock, the side chain of **7** is preorganized in an *anti-*χ conformation that allows optimal interaction of the carboxy group in the carboxylate binding region of CT. The same conformation appears to be attained by **6** in its bound state, but it has to be selected from a pool of different rotamers that are simultaneously present in solution. NMR analysis of the bound state of the ligands also reveals that the phenyl ring of **7** is in close contact with the protein, as revealed by the intense signal of the aromatic protons in the STD spectrum of the CT:**7** complex. In contrast, the cyclohexyl group of **6** appears to make a much loser contact with the toxin. Thus, the preorganization effect and a more efficient van der Waals interaction between the side-chain substituent and the protein appear to concur in determining the high affinity of **7** for CT.

The phenyl ring–GalNAc stacking interaction that we have observed in **7** has been described here for the first time as an element of a conformation lock in the structure of a sugar mimic. This kind of sugar–aromatic interaction, which is very well described in the context of carbohydrate/protein complexes[20–24] may have a broader application, which we intend to explore, as an element in conformation-based design of sugar mimics. Additionally, it has been reported that the presence of the hydrophobic ceramide moiety may influence the head-group presentation of the glycan[30] and may even influence the binding to cholera toxin.[31] Thus, although this report has focused on the importance of the oligosaccharidic part, further studies in our groups are paying attention to the importance of the lipid chain for the interaction under different experimental conditions.

Experimental Section

NMR spectroscopy experiments: NMR spectra were recorded at 25–30 °C in D_20 on Varian Unity 500 MHz and Bruker Avance 400 and 500 MHz spectrometers. For the experiments with the free ligand, the compound was dissolved in D_2O and the solution was degassed witha stream of argon. COSY, TOCSY, and HSQC experiments were performed by using the standard sequences. 2D T-ROESY experiments were performed with mixing times of 300 and 500 ms. The strength of the 180 pulses during the spin-lock period was attenuated 4 times with respect to that of the 90 hard pulses (between 7.2 and 7.5 μs). In order to deduce the interproton distances, relaxation matrix calculations were performed by using software written inhouse which is available from the authors upon request.[32] For the bound ligands, STD and TR-NOE experiments were performed as previously described.[8] First, the B chain of cholera toxin was subjected to 2 cycles of freeze–drying with D_2O to remove traces of H_2O. It was then transferred in solution to the NMR spectroscopy tube to give a final concentration of approximately 0.1–0.2 mM. TR-NOESY experiments were performed with mixing times of 100, 200, and 300 ms, for molar ratios of ligand/protein between 15:1 and 50:1. No purging spin-lock period to remove the protein background signals was employed. First, in all cases, line broadening of the sugar protons was monitored after the addition of the ligand. STD experiments were carried out by using the method proposed by Meyer, Peters, and their respective co-workers.[26–28] No saturation of the residual HDO signal was employed and, again, no spin-lock pulse was employed remove the protein background signals. In our hands, the use of a spin-lock period induced artifacts in the difference spectrum. The theoretical analysis of the TR-NOE contacts of the sugar protons was performed according to the protocol employed by London, with a relaxation matrix with exchange as described.[8] Different exchange-rate constants, k, defined as $pf \cdot k = K_{-1}$ (where pf is the fraction of the free ligand), and leakage relaxation times were employed to obtain the optimal match between the experimental and theoretical results for the intraresidue H-1/H-3 and H-1/H-5 cross-peaks of the Gal and GalNAc moieties for the given protein/ligand ratio. Normalized intensity values were used since they allow correcting for spin-relaxation effects. The overall correlation time, τ_c, for the free state was always set to 0.15 ns and the τ_c for the bound state was estimated as 15 ns according to the molecular weight of the toxin ($\tau_c = 10–12 \times M_W$). To fit the experimental TR-NOE intensities, exchange-rate constants, k, between 100–1000 s^{-1} and external relaxation times, ρ^*, for the bound state of 0.5, 1, and 2 s were tested. Optimal agreement was achieved when $k = 150\ s^{-1}$ and $\rho^* = 1$ s.

TR-ROESY experiments were also carried out to exclude spin-diffusion effects. A continuous-wave spin-lock pulse was used during the 250 ms mixing time. Key NOE contacts were shown to be direct cross-peaks, since they showed different signs to diagonal peaks. In some cases, they allowed the detection of intra-Gal and intra-GalNAc H-1/H-4 and H-1/H-6 cross-peaks that were due to spin diffusion.

Computational methods

Conformation search and dynamics of isolated 6 and 7: The calculations were performed by using the MacroModel/Batchmin[33] package (version 7.0) and the AMBER* force field. Kolb's parameters were used for the hydroxy acid moiety.[25] Bulk water solvation was simulated by using MacroModel's generalized Born GB/SA continuum solvent model.[34] The conformation searches were carried out by using 20,000 steps of the usage-directed MC/EM procedure according to previously established protocols.[35,19] Extended nonbonded cut-off distances (a van der Waals cut-off of 8.0 Å and an electrostatic cut-off of 20.0 Å) were used.

For the MC/SD[36] dynamic simulations, van der Waals and electrostatic cut-offs of 25 Å, together with a hydrogen-bond cut-off of 15 Å, were used. The dynamic simulations were run with the AMBER* all-atom force field. Charges were taken from the force field (all-atom option). The same degrees of freedom of the MC/EM searches were used in the MC/SD runs. All simulations were performed at 300 K, with a dynamic time step of 1 fs and a frictional coefficient of 0.1 ps^{-1}. Typically, 2 runs of 5 ns each were performed, with 2 conformations of the substrates as the starting point; these conformations differed at the hydroxy acid linkage and were selected from the MC/EM outputs. The Monte Carlo acceptance ratio was about 4%, and each accepted MC step was followed by an SD step. Structures were sampled every 1 ps and saved for later evaluation. Convergence was checked by monitoring both energetic and geometrical parameters.

Conformation search (MC/EM) of the LT complexes: The conformation searches were carried out by using the usage-directed MC/EM procedure, with slight variations of the protocol used in the study of the LT/psGM1 complex.[4] In brief, the starting structure for LT/**7** was obtained by superimposing the conformation of **7** that exhibits the best fit with the NOE data (conformer c in Figure 5) on the psGM1 ligand in our model of the LT:psGM1 complex by using the galactose coordinates. This "docking" step was followed by substructure energy minimization. The starting struture of the LT/**6** complex was obtained from the LT/**7** complex by graphically converting the phenyl ring into a cyclohexyl group.

The explicit torsional variables were the same as those used for the free-state calculations, that is, the Gal–GalNAc and Gal–CHD anomeric linkages, the C-5–C-6 bonds of Gal and GalNAc, and the five bonds of the hydroxy acid moiety. Furthermore, the ligand was allowed to rotate (max

180°) and translate (max. 1 Å) within the binding site (MOLS command of Batchmin). 10000 MC/EM steps were performed. Bulk water solvation was simulated by using the GB/SA model. Five crystallographic water molecules were retained, as previously described.[4,35] All calculations were carried out on a B2 (B+B(+1)) dimer. Only the ligand and a shell of residues surrounding the binding site of LT were subjected to energy minimization. All the residues within 6 Å of the sugars were completely included in the shell. An all-atom treatment was used for the ligand and for the aromatic residues of the protein. The rest of the toxin was treated with a united-atom model. The ligand and all of the binding site polar hydroxy and amino hydrogen atoms were unconstrained during energy minimization. All other atoms that belonged to the substructure being minimized were constrained to their crystallographic coordinates by parabolic restraining potentials that increased with the distance from the sugar substrate. The following force constants were used: 100 kJ Å^{-2} for atoms within 0–3 Å of any atom of the ligand; 200 kJ Å^{-2} for atoms within 3–4 Å; 400 kJ Å^{-2} for atoms within 4–5 Å. The periphery of the restrained structure was checked with the EdgeD command of MacroModel, and isolated atoms were included to avoid incomplete functional groups. All other atoms were ignored.

MC/SD dynamics of the LT:ligand complexes: The simulations were carried out by using the same substructure and explicit MC variables described above, but with the lowest energy conformation from the MC/EM search as the starting point. Extended nonbonded cut-offs were employed (van der Waals and electrostatic cut-off of 25 Å, hydrogen-bond cut-off of 15 Å). The simulations were performed for 1 ns, at 300 K, with a dynamic time step of 1 fs and a frictional coefficient of 0.1 ps^{-1}. Structures were sampled every 2 ps and saved for later evaluation.

Acknowledgments

The project was supported by the Azioni Integrate program between Italy and Spain, and the European programs COST-D13 and "Improving Human Potential" under contract HPRNCT-2002-00173 (Glycidic Scaffolds Network). I.S.-M. acknowledges a Marie Curie Fellowship from the European Community program 'Improving Human Potential' under contract HPMT-CT-2001-00293. The Madrid group also acknowledges the Ministery of Science and Technology of Spain for funding (Grant BQU2003–03550-C01).

[1] P. Sears, C. H. Wong, *Angew. Chem.* **1999**, *111*, 2446–2471; *Angew. Chem. Int. Ed.* **1999**, *38*, 2300–2324, and references therein.
[2] C.-L. Schengrund, N. J. Ringler, *J. Biol. Chem.* **1989**, *264*, 13233–13237.
[3] E. A. Merritt, S. Sarfaty, F. van den Akker, C. L'Hoir, J. A. Martial, W. G. J. Hol, *Protein Sci.* **1994**, *3*, 166–175; E. A. Merrit, T. K. Sixma, K. H. Kalk, B. A. M. Van Zanten, W. G. J. Hol, *Mol. Microbiol.* **1994**, *13*, 745–753; E. A. Merrit, S. Sarfaty, M. G. Jobling, T. Chang, R. K. Holmes, W. G. J. Hol, *Protein Sci.* **1997**, *6*, 1516–1528.
[4] A. Bernardi, A. Checchia, P. Brocca, S. Sonnino, F. Zuccotto, *J. Am. Chem. Soc.* **1999**, *121*, 2032–2036.
[5] A. Bernardi, G. Boschin, A. Checchia, M. Lattanzio, L. Manzoni, D. Potenza, C. Scolastico, *Eur. J. Org. Chem.* **1999**, 1311–1317.
[6] A. Bernardi, L. Carrettoni, A. Grosso Ciponte, D. Monti, S. Sonnino, *Bioorg. Med. Chem. Lett.* **2000**, *10*, 2197–2200.
[7] D. Arosio, S. Baretti, S. Cattaldo, S. Potenza, A. Bernardi, *Bioorg. Med. Chem. Lett.* **2003**, *13*, 3831–3834.
[8] A. Bernardi, D. Potenza, A. M. Capelli, A. García-Herrero, F. J. Cañada, J. Jiménez-Barbero, *Chem. Eur. J.* **2002**, *8*, 4597–4612.
[9] A. A. Bothner-By, R. Gassend, *Ann. N.Y. Acad. Sci.* **1973**, *222*, 668–676.
[10] P. L. Jackson, H. N. Moseley, N. R. Krishna, *J. Magn. Reson. Ser. B* **1995**, *107*, 289–292; V. L. Bevilacqua, D. S. Thomson, J. H. Prestegard, *Biochemistry* **1990**, *29*, 5529–5537; V. L. Bevilacqua, Y. Kim, J. H. Prestegard, *Biochemistry* **1992**, *31*, 9339–9349; H. Kogelberg, D. Solís, J. Jiménez-Barbero, *Curr. Opin. Struct. Biol.* **2003**, *13*, 646–653;
[11] A. Schon, E. Freire, *Biochemistry* **1989**, *28*, 5019–5024.
[12] M. B. Khalil, M. Kates, D. Carrier, *Biochemistry* **2000**, *39*, 2980–2988.
[13] K. Bock, J. O. Duus, *J. Carbohydr. Chem.* **1994**, *13*, 513–543.
[14] D. Neuhaus, M. P. Williamson, *The NOE Effect in Structural and Conformational Analysis*, VCH, New York, **1989**.
[15] T. L. Hwang, A. J. Shaka, *J. Am. Chem. Soc.* **1992**, *114*, 3157–3158.
[16] *NMR Spectroscopy of Glycoconjugates* (Eds.: J. Jiménez-Barbero, T. Peters), VCH, Weinheim, **2002**.
[17] J. Dabrowski, T. Kozar, H. Grosskurth, N. E. Nifant'ev, *J. Am. Chem. Soc.* **1995**, *117*, 5534–5539.
[18] A. Bernardi, D. Arosio, L. Manzoni, D. Monti, H. Posteri, D. Potenza, S. Mari, J. J. Barbero, *Org. Biomol. Chem.* **2003**, *1*, 785–792.
[19] P. Brocca, A. Bernardi, L. Raimondi, S. Sonnino, *Glycoconjugate J.* **2000**, *17*, 283–299.
[20] N. K. Vyas, *Curr. Opin. Struct. Biol.* **1991**, *1*, 732–740.
[21] F. A. Quiocho, *Biochem. Soc. Trans.* **1993**, *21*, 442–448.
[22] W. I. Weis, K. Drickamer, *Annu. Rev. Biochem.* **1996**, *65*, 441–473.
[23] S. Elgavish, B. Shaanan, *J. Mol. Biol.* **1998**, *277*, 917–932.
[24] J. Jimenez-Barbero, J. L. Asensio, F. J. Cañada, A. Poveda, *Curr. Opin. Struct. Biol.* **1999**, *9*, 549–555.
[25] H. C. Kolb, B. Ernst, *Chem. Eur. J.* **1997**, *3*, 1571–1578.
[26] M. Meyer, B. Meyer, *Angew. Chem.* **1999**, *111*, 1902–1906; *Angew. Chem. Int. Ed.* **1999**, *38*, 1784–1788.
[27] J. Klein, R. Meinecke, M. Meyer, B. Meyer, *J. Am. Chem. Soc.* **1999**, *121*, 5336–5337.
[28] M. Vogtherr, T. Peters, *J. Am. Chem. Soc.* **2000**, *122*, 6093–6099.
[29] J. L. Asensio, F. J. Cañada, J. Jimenez-Barbero, *Eur. J. Biochem.* **1995**, *233*, 618–630.
[30] D. Roy, C. Mukhopadhyay, *J. Biomol. Struct. Dyn.* **2002**, *19*, 1121–1132.
[31] B. Lanne, B. Schierbeck, J. Angstrom, *J. Biochem.* **1999**, *126*, 226–234.
[32] A. Poveda, J. L. Asensio, M. Martín-Pastor, J. Jimenez-Barbero, *J. Biomol. NMR* **1997**, *10*, 29–43.
[33] F. Mohamadi, N. G. J. Richards, W. C. Guida, R. Liskamp, M. Lipton, C. Caufield, G. Chang, T. Hendrickson, W. C. Still, *J. Comput. Chem.* **1990**, *11*, 440–467.
[34] W. C. Still, A. Tempzyk, R. Hawley, T. Hendrickson, *J. Am. Chem. Soc.* **1990**, *112*, 6127–6129.
[35] A. Bernardi, L. Raimondi, F. Zuccotto, *J. Med. Chem.* **1997**, *40*, 1855–1862.
[36] F. Guarnieri, W. C. Still, *J. Comput. Chem.* **1994**, *15*, 1302–1310.

Received: January 26, 2004
Revised: May 3, 2004
Published online: July 27, 2004

